Journal of Materials Science and Chemical Engineering, 2026, 14(6), 42-66
https://www.scirp.org/journal/msce
ISSN Online: 2327-6053
ISSN Print: 2327-6045

Interactive Effects of API Gravity and Storage Geometry on Short-Term Volume Retention of Selected Polar and Nonpolar Organic Liquids

Gideon Mudiaga Efetobor[1], Idongesit Effiong Ekpo[2*], Ikodia Orji[2], Achugasim Ozioma[2], Pereware Adowei[2]

[1]Department of Chemical/Petroleum Technology, University of Port Harcourt, Port Harcourt, Nigeria
[2]Department of Pure and Industrial Chemistry, Faculty of Science, University of Port Harcourt, Port Harcourt, Nigeria
Email: gideonefetobor@gmail.com, *idongesit.ekpo@uniport.edu.ng, ikodiya.orji@uniport.edu.ng, ozioma.achugasim@uniport.edu.ng, pereware.adowei@uniport.edu.ng

How to cite this paper: Efetobor, G.M., Ekpo, I.E., Orji, I., Ozioma, A. and Adowei, P. (2026) Interactive Effects of API Gravity and Storage Geometry on Short-Term Volume Retention of Selected Polar and Nonpolar Organic Liquids. *Journal of Materials Science and Chemical Engineering*, **14**, 42-66.
https://doi.org/10.4236/msce.2026.146003

Received: May 13, 2026
Accepted: June 22, 2026
Published: June 25, 2026

Copyright © 2026 by author(s) and Scientific Research Publishing Inc.
This work is licensed under the Creative Commons Attribution International License (CC BY 4.0).
http://creativecommons.org/licenses/by/4.0/
Open Access

Abstract

The interactive effects of API gravity and storage geometry on the volume retention of selected polar and nonpolar organic liquids (ethanol, methanol, low-molecular-weight crude oil [LCO], and natural gas liquids [NGL]) were investigated in this study over 7 days of evaporative storage. The storage systems used for monitoring the process were shaped into five different geometries (horizontally cylindrical, vertically cylindrical, cuboidal, spherical, and conical), and the liquids used in this study were characterized by API gravity, dipole moment, standard enthalpy of vaporization, vapor pressure, and interfacial evaporation descriptors. The results showed that liquid retention was governed by a competitive interplay among volatility, cohesive intermolecular attraction, gas-phase mass transfer, and vessel geometry. The consistent poor retention of NGL was attributed to its high API gravity, low effective cohesive energy, and very high vapor pressure. At the same time, ethanol and LCO exhibited the highest retention due to their lower volatility and greater resistance to evaporation. The polar compounds showed that ethanol retained more volume than methanol. However, both compounds have a close range of API gravities and dipole moments, indicating that the enthalpy of vaporization and vapor pressure were more decisive than polarity alone. The role of geometry was enormous as the conical vessel had the highest cumulative retention, while the spherical vessel had the least. Therefore, short-term storage losses are controlled not by API gravity alone, but by the combined effects of thermodynamic properties and storage geometry, with clear implications for reducing evaporation losses and for storage design in the process industries.

Keywords

API Gravity, Storage Geometry, Polarity, Organic Liquid, Evaporation

1. Introduction

Evaporative shrinkage leads to volume loss; the rate of volume loss is governed by both molecular thermodynamics and external mass transfer. API gravity indirectly affects evaporative shrinkage in hydrocarbon liquids by serving as a bulk indicator of the extent of weight of the liquids, as well as the distribution of volatile components in the substance. Liquids with higher true vapour pressures with numerous amounts of low boiling components are usually identified with high API values and have the potential to exhibit greater evaporative shrinkage generally; evaporative shrinkage of liquids is fundamentally governed by vapour pressure, composition, temperature, and mass-transfer conditions rather than API gravity alone [1]-[6].

The polarity influences intermolecular cohesion, enthalpy of vaporisation, vapour pressure, and non-ideal phase behaviour, as a result affecting shrinkage in liquids. Observed shrinkage rate is controlled by gas-phase diffusion, convection, temperature, and exposed surface area. Dipole moment describes polarity for pure molecular liquids; though dipole moment does not have a single property for multicomponent petroleum liquids; for such mixtures, polarity is better described qualitatively or through bulk properties rather than by one fixed molecular dipole moment. Studies have shown that polarity is not a stand-alone indicator of evaporation shrinkage, but influences it through other factors: cohesive interactions, non-ideality, and vapor pressure [7]-[10].

Previous studies have provided comprehensive explanations of the effects of volatility, tank losses, and mass transfer on evaporative shrinkage. However, fewer studies have emphasized the effects of polarity and API gravity across multiple storage geometries, as this study will do. This work will evaluate the effects of API gravities and polarities on the volume reduction of processed organic liquids via evaporative shrinkage. It will also investigate the dependence of these molecular thermodynamic parameters on varied headspaces (The exposed liquid-air interfacial areas are considered a geometric proxy for the influence of headspaces on evaporative shrinkage) created by various geometries of storage vessels.

2. Related Works

Studies have examined how the evaporation behaviour of liquid mixtures can be quantified using a simple, low-cost experimental approach to measure evaporation rates [5]. The paper further shows that evaporation-rate data can be used to estimate flash point, linking volatility directly to fire and handling safety.

Its contribution is that evaporation kinetics are not only a transport phenomenon but also a practical safety indicator for storage, handling, and risk assessment of volatile liquid mixtures.

Work was carried out on the systematic review of evaporation loss and near-field diffusion of volatile organic compounds (VOCs) from petrochemical storage tanks by putting together evidence from 200 English and Chinese publications published between 1972 and April 2025 [11]. Considered in this review were: evaluation of theoretical models, investigation of experimental and numerical methods, consideration of major influencing factors, and assessment approaches of losses due to evaporation for tank emissions. This study also considered roof tanks (floating, internal floating, and dome), whose source composition, toxic/flammable species, and local diffusion behaviour were examined around the external tanks under varying wind and obstacle conditions. The core value for this work, in relation to the present study, is that a clearer understanding of mechanisms of evaporation and local VOC dispersion is essential for improving loss prevention, exposure control, and emergency response in petrochemical storage operations.

Studies have developed a numerical calculation method to simulate oil-vapour diffusion and breathing losses in a dome-roof tank under solar radiation, using n-hexane as a representative light oil.

It was clarified that the coupled heat- and mass-transfer mechanisms in tank vapour space show that both breathing loss and loss rate are highest in summer [12]. Among the findings here was that breathing losses increase with liquid level, and loss rates varied with the combined effects of gas temperature and liquid height. This establishes that solar loading and storage conditions strongly control vapour generation and evaporative loss in fixed-roof petroleum tanks.

A work reviewed evaporation driven by convection from open liquid surfaces, synthesizing the main governing mechanisms and the influence of liquid-vapour conditions on evaporation rate [13]. The paper shows that evaporation is controlled by variables such as gas pressure, temperature, humidity, flow velocity, turbulence, liquid properties, surface temperature, and exposed surface area. It also compiles evaporation-rate correlations from the literature, including 32 for natural convection, 7 for mixed convection, and 116 for forced convection, together with their ranges of validity. The study is related to this work as it establishes evaporation as a coupled heat-and-mass-transfer process in which convection and exposed geometry strongly influence liquid-loss behaviour.

In this study, the liquids with the highest and lowest retained volumes in storage vessels will be investigated, and the molecular thermodynamics will be studied.

Variation in API gravity and polarity of the liquids will be considered to investigate their effects on the liquids' evaporation patterns in the study. The effects of the vessels' design on the selected fluid properties, as they relate to volume retention after evaporation, are also considered. The defensible framework for volatility distribution and polarity-dependent intermolecular effects is also considered.

The studies by [14] and [15] are considered in this study as conceptual, not evidentially equivalent. [14] showed that, for a fixed porous material, salt concentration, and liquid volume, the size of the evaporative surface area strongly affects drying kinetics and the pattern of salt crystallisation. By applying truncated-cone-

shaped sandstone and NMR-based tracking of ion concentration, it was deduced that different exposed surfaces alter liquid and ion transport and the balance between efflorescence and subflore, Gas-phase diffusion/convective mass-transfer models.

Observed shrinkage is not controlled by thermodynamics alone. NIST's fire-dynamics reference expresses liquid mass loss with a gas-side mass-transfer model.

So even if two liquids differ in polarity, the measured shrinkage can change substantially with surface area, vessel geometry, Reynolds number, Schmidt number, airflow, and diffusion coefficient. This is why "polarity effect" is often clearer in controlled isothermal comparisons than in raw storage experiments. This work is related to the present study because it established that the controlling variable in mass transfer and deposit formation is the surface geometry during evaporation and that larger damaged or exposed regions may accelerate material deterioration over time.

According to the research carried out, a model and analysis of the various tank geometries and relief pressure on liquid hydrogen (LH_2) boil-off losses was conducted, which is relevant to the present study. LH_2 boil-off losses were modelled using the BoilFAST simulation platform, incorporating realistic heat-transfer mechanisms and equations of state, and were validated against NASA data. The study compares horizontal, vertical, spherical, and cuboid tank geometries and shows that relief pressure strongly influences liquid-volume loss, much more than fill level. Across the tested designs, the spherical tank consistently gave the lowest boil-off losses, while the cuboid tank showed the highest losses. The study is related to the present study because it identified important variables governing evaporative loss in cryogenic liquid storage systems, such as storage geometry and pressure control strategy [15].

3. Materials and Methods

3.1. Sampling

The four organic liquids used for this study, ethanol, methanol, low-molecular-weight crude oil (LCO), and natural gas liquids (NGL), were obtained in two different ways: ethanol and methanol as analytical reagents produced by Sigma-Aldrich. At the same time, LCO and NGL were obtained as processed products from upstream oil and gas operations in Nigeria.

3.2. Analysis of API Gravity of Organic Liquids

The API thermohydrometer was used to measure the API gravities of the Organic liquids at ambient conditions, using ASTM D1298-24. A correction table was used to convert the API gravity data from ambient conditions to 60˚F, and Equations (1) and (2) were used to evaluate the specific gravities (SG) and densities of the organic liquids [16] [17].

$$\text{API gravity at } 60^\circ\text{F}\left(^\circ\text{API}\right) = \frac{141.5}{\text{Specific gravity}\left(\text{S.g}\right)\text{ at } 60^\circ\text{F}} - 131.5 \quad (1)$$

$$\rho_{\text{substance}} = \text{S.g} \times \rho_{\text{water}} \tag{2}$$

where:

$\rho_{\text{substance}}$ is the density of the organic liquid in kg·m^{-3}.

ρ_{water} is the density of equal volume of water in kg·m^{-3}.

S.g is the specific gravity of the organic liquid at 60˚F (dimensionless).

3.3. Determination of Dipole Moment of Organic Liquids

This was carried out for the alcohols. The samples were homogeneous, clean liquids, and the laboratory temperature was maintained at 24˚C. The samples were left for 24 hours to attain the laboratory conditions. The N1501A Dielectric Probe, which used a coaxial probe method and was manufactured by Keysight Technologies, was calibrated with air and water, then used for the detection of dielectric constant; the static relative permittivity, ε_r, of the liquid at a fixed temperature using dielectric spectroscopy. The refractive index (n), density (ρ), molar mass (M), and temperature (T) were determined and recorded.

The total molar polarization, P_m, and molar refraction (R_m) were calculated using Equation (3) and Equation (4). The orientational polarization, P_o, in Equation (5) was obtained by subtracting the induced polarization term from the total polarization. The dipole moment (μ) was derived by substituting the orientational polarization (Equation (5)) into the Debye relation (Equation (6)). The resulting μ in Equation (7) is the effective liquid-phase dipole moment in coulomb meter (C·m), which can be converted to Debye (D) using Equation (8) [7] [18] [19].

$$P_m = \frac{M}{\rho}\left(\frac{\varepsilon_r - 1}{\varepsilon_r + 2}\right) \tag{3}$$

$$R_m = \frac{M}{\rho}\left(\frac{n^2 - 1}{n^2 + 2}\right) \tag{4}$$

$$P_o = P_m - R_m \tag{5}$$

$$P_o = \frac{N_A \mu^2}{9\varepsilon_0 k_B T} \tag{6}$$

$$\mu = \sqrt{\frac{9\varepsilon_0 k_B T P_o}{N_A}} \tag{7}$$

$$1\,\text{D}(\text{Debye}) = 3.33564 \times 10^{-30}\ \text{C}\cdot\text{m}(\text{coulomb metre}) \tag{8}$$

where:

ε_r is the static relative permittivity (dielectric constant) of the liquid.

n is the refractive index of the liquid, typically measured at an optical frequency.

ρ is the density of the liquid at the measurement temperature.

M is the molar mass of the liquid.

T is the absolute temperature in kelvin.

P_m is the total molar polarization.

R_m is the molar refraction or induced/electronic polarization term.

P_o is the orientational polarization associated with permanent dipoles, in m^3·mol^{-1}.

μ is the Permanent dipole moment estimated for the liquid phase, Debye (D) or C·m.

N_A, k_B, and ε_0 are Avogadro constant, Boltzmann constant, and vacuum permittivity, respectively.

3.4. Design Basis and Sizing Criteria of Storage Vessels

The storage vessels used in this study were bench-scale vessels intentionally fabricated in multiple geometries to isolate the effect of vessel geometry on measured liquid shrinkage.

Even when the vessels were made from small containers with different geometries, the design philosophy was predominantly based on storage tank standards, with an emphasis on integrity, dimensional control, and safe containment of liquids [20].

The storage vessels were produced with a volume of 1.5 L ± 0.2 L, which ensured sufficient liquid volume to withstand repeated volume measurements and comparable shrinkage trends across geometries under identical ambient conditions.

The study evaluated five vessel geometries: Vertical cylindrical, Horizontal cylindrical, Spherical, Conical, and Cuboidal vessels (**Figures 1(a)-(e)**, respectively). The five (5) vessels were designed with approximately equal venting dimensions. The rectangular vent opening is 32 mm × 10 mm, as shown in **Figure 1(f)**.

Figure 1. Pictures of fabricated storage vessels: (a) vertical cylindrical; (b) horizontal cylindrical; (c) spherical; (d) conical; (e) cuboidal; (f) upper section of cuboidal vessel.

Vessels were fabricated strictly according to the CAD drawings to maintain dimensional repeatability across geometries. After fabrication, vessels were checked for dimensional conformity (critical internal dimensions) and capacity conformity to the target range of approximately 1.5 L ± 0.2 L, before shrinkage experiments. Also, joints and seams were verified to be leak-tight before use [21] [22].

Although this work is laboratory-scale, storage-tank standards provide a defensible framework for reporting methodology (materials/design/fabrication/inspection mindset). Recent literature continues to highlight that code-based procedures (e.g., API-type approaches) are often complemented by advanced analyses (e.g., nonlinear dynamic checks).

3.5. Calibration of Storage Vessels

The five storage vessels were calibrated using the gravimetric liquid-fill method. Each vessel was calibrated individually, after being cleaned, dried, and placed on a level surface. Distilled water was used as the calibration liquid. For each point in each vessel, distilled water was weighed, and the corresponding liquid height and diameter were recorded after the liquid surface had stabilized at 22˚C - 25˚C. The volume at the point was calculated from the measured mass and density using the equation for specific geometrical volume. The calibration was performed at 20 mL intervals from 400 - 1000 mL, and the procedure was repeated in triplicate for each vessel. Mean volume-height data were used to construct calibration curves for the different vessel geometries [23].

3.6. Measurement of Volumes of Organic Liquids in Storage Vessels

Liquid quantity in each vessel was determined from the measured liquid level (depth) and a vessel-specific calibration chart (capacity table). In manual dipping, a calibrated rule/tape is lowered to a fixed reference (datum), and the wetted line indicates the liquid level. The innage gauge method here is also referred to as manual dipping. The observed level was then converted to volume using the capacity table prepared for each vessel. This approach follows established manual tank-gauging practice for petroleum and related liquids. The liquid measurement and other laboratory experiments were performed under laboratory conditions of 22˚C - 25˚C, 48% - 50% relative humidity in a mechanically ventilated laboratory of 6 air changes per hour (ACH) maintained under negative pressure. The major apparatus used is as follows [24]:

i) ≤1 mm resolution graduated stainless-steel rule or steel sounding tape.

ii) A weighted small bob to ensure vertical alignment and contact with the datum.

iii) A gauging paste to indicate oil level and sharpen the liquid contact line, thereby reducing meniscus-reading ambiguity.

iv) Vessel calibration chart for each vessel geometry; this was used to convert each measured depth to volume.

After transfer, each vessel was allowed to stand briefly to minimize sloshing and to obtain a stable free surface before gauging (important for repeatable level readings).

Consistent reference-point control was enhanced as all depth readings were taken to the exact vessel bottom. This was critical because any "zero-offset" between the gauging reference and the calibration table reference introduces systematic bias in volume results.

A thin, uniform layer of oil paste was applied to the lower portion of the rule/tape over the expected wetting zone.

The measuring tape was lowered vertically until the bob just reached the bottom of the vessel.

The measuring tape was carefully withdrawn, and the measurement of the sharp change in the paste (wetted boundary) was read as the innage depth (h) to the nearest graduation.

Manual gauging steps and key influences (reference point, tape handling, bob effects) are consistent with recognized petroleum manual-gauging guidance.

The readings were taken in triplicate (without changing the reference point), and the mean depth was recorded as the daily level for that vessel.

Measured depth (h) was converted to volume (V) using the vessel-specific capacity calibration chart developed for each geometry. Equations (9) and (10) show the calculation of the daily loss in volume in the storage [25] [26] (International Organization for Standardization, 2022; International Organization for Standardization, 2023). 1000 mL (being the initial volume, V_0) of each organic liquid was measured into each storage vessel, and the volume to depth equivalent was evaluated.

$$\Delta V_t = V_0 - V_t \tag{9}$$

$$\%\text{Loss} = \frac{V_0 - V_t}{V_0} \times 100 \tag{10}$$

where:

V_0 is the initial volume at time t equal to zero in ml.

V_t is the volume at t not equal to zero in ml.

3.7. Models and Equations

3.7.1. Intermolecular Force Theory

Considering molecules of similar size, an increase in polarity usually strengthens dipole-dipole attraction, and hydrogen bonding strengthens cohesion even more. Stronger cohesion means more energy is needed for molecules to escape the liquid, so evaporation tends to slow and shrinkage tends to decrease. The alcohol and methanol used for this study are analytical grade, so the standard enthalpy of vaporization (ΔH_{vap}°) stated in the National Institute of Standards and Technology (NIST) data sheet at 298.15 K was used. The model used the intermolecular force, or cohesive energy, to evaluate the molar energy required to convert a substance from liquid to vapour using the standard enthalpy of vaporization [5] [13]

[27] [28].

Equation (11) shows that ΔH_{vap}° as a thermodynamic state function, it can be obtained from the difference between the molar enthalpy of the gas and liquid and cohesive internal energy (U_{coh}) derived from ΔH_{vap}° as its difference with the expansion work contribution as shown in Equation (12), giving rise to the cohesive energy density (*CED*) in Equation (13). Equation (14) shows the Hildebrand solubility parameter (δ). δ implies that larger ΔH_{vap}° values generally correspond to larger cohesion-related solvent parameters.

$$\Delta H_{vap}^{\circ} = H_g^{\circ} - H_l^{\circ} \tag{11}$$

$$U_{coh} \approx \Delta H_{vap}^{\circ} - RT \tag{12}$$

$$CED = \frac{\Delta H_{vap}^{\circ} - RT}{V_m} \tag{13}$$

$$\delta = \sqrt{\frac{\Delta H_{vap}^{\circ} - RT}{V_m}} \tag{14}$$

where:

H_g° is the standard molar enthalpy of the vapor.

H_l° is the standard molar enthalpy of the liquid.

U_{coh} is the liquid cohesive energy per mole.

R is the universal gas constant.

T is the absolute temperature.

CED is the cohesive energy density.

V_m is the molar volume of the liquid.

δ is the Hildebrand solubility parameter.

3.7.2. Measurement of the Vapor Pressure of Organic Liquids

The Clausius-Clapeyron model, as given in Equation (15), relates the equilibrium vapor content to temperature and the latent heat. This model explains why more volatile liquids evaporate faster. The equilibrium vapor pressure rises with temperature and depends on the latent heat of vaporization [1]:

$$\ln \frac{P_{sat}}{P^o} = -\frac{\Delta H_{vap}}{RT} + C \tag{15}$$

where:

P_{sat} is the saturation vapor pressure of the liquid in Pa.

P^o is the = reference pressure in Pa (1 Pa).

ΔH_{vap} is the enthalpy of vaporization in J·mol^{-1}.

R is the universal gas constant in J mol^{-1}·K^{-1} (8.314 J·mol^{-1}·K^{-1}).

T is the absolute temperature in K.

C is the integration constant.

The true vapour pressure of the organic liquids that are pure solvents (ethanol and methanol) was measured using ASTM D2879-23. The liquid sample was loaded into a KD2879 Isoteniscope Pressure Manometer (a constant-volume glass

apparatus designed to minimize composition change during testing) manufactured by Koehler Instrument Company, Inc. Dissolved and entrained fixed gases were removed by heating a thin sample layer under reduced pressure, with minimal loss of volatile components. The process was carried out at 30˚C; the sample vapor was balanced against nitrogen gas pressure. The pressure at which both compartments gave equal pressure was noted with the manometer reading. The vapour pressure at the measured temperature was taken as the equilibrium pressure. The process was repeated in triplicate, and the average value was recorded [29].

Raoult's law, as expressed in Equation (16), is a better model for describing evaporation in component mixtures. Here, the total vapor pressure depends on the volatility of the individual fractions [30]:

$$P = \sum_i x_i \gamma_i P_i^{sat} \tag{16}$$

where:

P is the total equilibrium vapor pressure of the liquid mixture, with units in Pa.

$\sum$ is the summation sign, meaning the contributions of all components in the mixture are added together.

x_i is the liquid-phase mole fraction of component i, unit is dimensionless.

γ_i is the activity coefficient of the component i in the liquid phase. It corrects for non-ideal behaviour; its unit is dimensionless.

P_i^{sat} is the saturation vapor pressure of the pure component i at the system temperature; unit in Pa.

i is the component index identifying each substance in the mixture; it is without a unit.

The two samples that are mixtures (NGL and LCO) were analysed for their vapour pressure using ASTM D6377-20 using the IP 481 eralytics eravap vapour pressure instrument manufactured by the eralytics GmbH company [31].

The sample was introduced into a test chamber and expanded to a specified vapor/liquid ratio (V/L), then held at 30˚C, and a reading was taken [32].

3.7.3. Interfacial Evaporation Model

At the liquid surface, evaporation can be described by a molecular-kinetic flux equation; an example is the Hertz-Knudsen-Langmuir equation. The modern review literature notes that the Hertz-Knudsen relation is widely used, but its empirical evaporation and condensation coefficients are not always easy to determine. In practical terms. The generic form of the Hertz-Knudsen equation is as shown in Equation (17) [1]:

$$J = \alpha \frac{\left(P_{sat} - P_v\right)}{\sqrt{2\pi MRT}} \tag{17}$$

where:

J is the net molar evaporation flux, unit is in mol $m^{-2} \cdot s^{-1}$.

α is the evaporation/accommodation coefficient is dimensionless.

P_{sat} ,m is the saturation vapour pressure of the evaporating liquid at the interface

temperature, unit is in Pa.

P_v is the actual vapour partial pressure of the evaporating species in the gas phase unit is Pa.

$(P_{sat} - P_v)$ is the driving force for net evaporation.

M is the molar mass of the evaporating substance unit is in kg·mol^{-1}.

R is universal gas constant unit is J·mol^{-1}·K^{-1} (8.314 J·mol^{-1}·K^{-1}).

T is the absolute temperature at the interface unit is in K.

π is the mathematical constant pi, it is dimensionless.

A few interpretation notes:

If $P_{sat} > P_v$, net evaporation occurs.

If $P_{sat} < P_v$, net condensation occurs.

If $P_{sat} = P_v$, the interface is at equilibrium and $J = 0$.

3.7.4. Gas-Phase Diffusion/Convective Mass-Transfer Models

Equations (18) and (19) describe gas-side controlled evaporation: Equation (18) gives the evaporation rate (mass loss rate), and Equation (19) shows how the mass-transfer coefficient (h_m) is obtained from the binary diffusion coefficient ($D_{\upsilon,g}$), a characteristic length (L), and convection through the Sherwood number (Sh). These models identify two factors contributing to increased evaporation: an increase in the exposed area as well as an increase in the mass transfer coefficient on the gas side. These equations show that evaporation becomes faster when vapor diffuses more readily through the gas phase or when convection increases. In other words, these equations link molecular diffusion and fluid-flow effects to the overall evaporation rate.

$$\dot{m}_{evap} = \frac{\mathrm{d}m_l}{\mathrm{d}t} = -Ah_m\rho_g\left(Y_{\upsilon,i} - Y_{g,\infty}\right) \tag{18}$$

$$h_m = \frac{Sh\,D_{\upsilon,g}}{LL} \tag{19}$$

The negative sign that is before A above indicates that the liquid mass decreases with time during evaporation. It also deduced that liquid loses mass at a rate ($\frac{\mathrm{d}m_l}{\mathrm{d}t}$) proportional to the exposed surface area (A), the gas-side mass-transfer coefficient (h_m), the gas density (ρ), and the driving force for evaporation, expressed as the difference between the equilibrium vapor mass fraction at the liquid surface and the vapor mass fraction in the bulk gas. The negative sign shows that the liquid mass decreases with time [3] [13].

where:

$\dot{m}_{evap}$ is the positive evaporation rate, kg·s^{-1}.

m_l is the liquid mass in kg.

t is time in s.

$\frac{\mathrm{d}m_l}{\mathrm{d}t}$ is the evaporation or mass-loss rate in kg·s^{-1}.

A is the exposed interfacial area in m^{-2}.

h_m is the mass-transfer coefficient in m·s^{-1}.

ρ_g is the gas density in kg·m^{-3}.

$Y_{\upsilon,i}$ is the equilibrium vapor mass fraction at the interface, which is dimensionless.

$Y_{g,\infty}$ is the vapor mass fraction in the bulk gas is dimensionless.

Sh is the Sherwood number is dimensionless.

$D_{\upsilon,g}$ is the binary diffusion coefficient of the liquid vapor in the surrounding gas in m^2·s^{-1}.

L is the characteristic length of the evaporating system, m.

Note that in practice, Sh is usually estimated from empirical correlations involving the Reynolds number (*Re*) and Schmidt number (*Sc*), both of which are dimensionless.

3.8. Statistical Analysis

The experiments for the liquid-geometry combination were conducted simultaneously in three independent runs, and each measurement was taken in triplicate.

Retained volume, percentage retention, percentage shrinkage, and percentage volume loss within the period of storage were calculated using the initial liquid volume (V_0 = 1000 ml) as the reference basis.

The main performance indicators were day-7 retained volume, day-7 shrinkage percentage, mean retained volume from days 2 - 7, and cumulative retention index, estimated as the area under the retained-volume-time curve using the trapezoidal method. These indices were used to compare the ability of each vessel geometry to minimize evaporative loss across the tested liquids.

Available replicate measurements involved the use of descriptive statistics: mean, standard deviation, coefficient of variation, range, and percentage change. Where values were obtained from single experimental profiles, the results were treated as descriptive performance indicators rather than independent statistical replicates. The four liquids were not treated as biological or experimental replicates because they differ in physicochemical properties, including API gravity, density, and volatility. Instead, liquid type and vessel geometry were considered fixed explanatory factors influencing evaporative shrinkage.

Prior to inferential comparison, data distribution and variance structure were assessed using the Shapiro-Wilk normality test and Levene's test for homogeneity of variance. When assumptions of normality and equal variance were met, one-way or two-way analysis of variance was used to compare shrinkage and retention indices across vessel geometries and liquid types. Where these assumptions were not satisfied, Welch's ANOVA or the Kruskal-Wallis test was applied as appropriate. Post-hoc comparisons were conducted using Tukey's test for equal variances, Games-Howell test for unequal variances, or Dunn's test with adjusted probability values for non-parametric comparisons.

For time-dependent volume-retention profiles, repeated-measures analysis or linear mixed-effects modelling was considered appropriate, with storage time as the repeated factor and liquid type and vessel geometry as fixed factors. Interac-

tion effects were examined to determine whether the influence of vessel geometry on evaporative shrinkage depended on liquid type or storage duration. Relationships between API gravity and evaporative performance indicators were assessed using Pearson correlation for normally distributed data or Spearman's rank correlation where normality was not satisfied.

Statistical significance was accepted at $p < 0.05$. In addition to probability values, effect sizes and 95% confidence intervals were reported where applicable [33]-[35].

4. Results and Discussion

4.1. Characterization of Organic Liquids

The API gravities of the liquids used for this study are shown in Figure 2; they increase in the order LCO < methanol < ethanol < NGL, with values ranging from 44.80 to 75.90 ˚API. The densities of these substances are expected to vary in the reverse order of their API gravities, as specified in Equation (1) and Equation (2) of the previous section. The difference between the API gravity of the liquid with the lowest value and that of the liquid with the highest value is sufficiently large to suggest substantial variations in the density-based index of the liquids for this study [36]. This observation is consistent with a lighter hydrocarbon character.

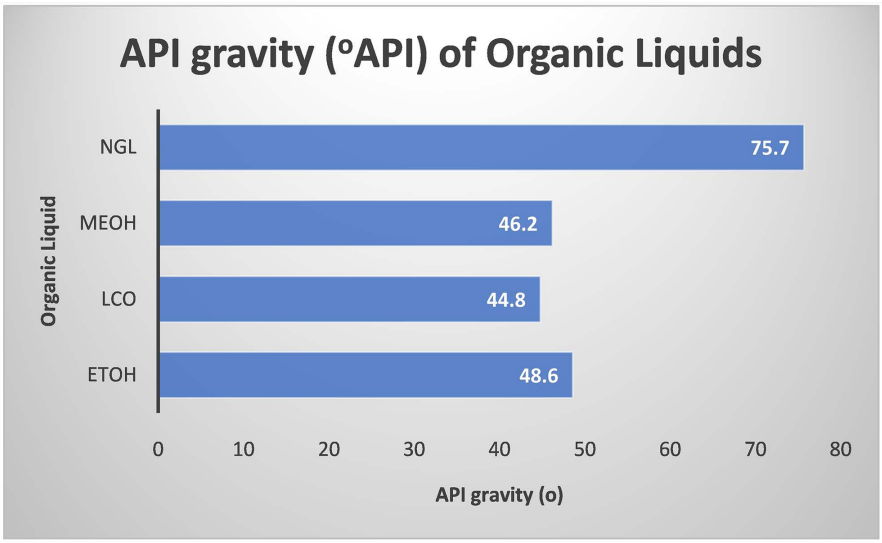

Figure 2. API gravity (˚API) of organic liquids.

The dipole moments of these liquids are shown in Table 1. These can be used to predict the increasing order of polarity of these liquids as LCO < NGL < ethanol < methanol; LCO consists of heavier and more complex hydrocarbons compared to NGL, which are dominated by short-chain alkanes. Both are largely nonpolar. While both ethanol and methanol are oxygenated organic compounds with a hydroxyl group (-OH), the latter has an alkyl group with fewer carbon atoms than

the former and so a higher dipole moment and polarity, as shown in Table 1. The presence of complex hydrocarbons in LCO and NGL makes it difficult to determine the actual dipole moments of these substances and infer that they have near-zero dipole moments and are nonpolar. Therefore, the four liquids may be commonly classified as organic liquids, as inferred in Table 2.

Table 1. Molecular thermodynamic properties of organic liquids.

Parameter	Ethanol	Methanol	LCO	NGL
Dipole Moment (D)	1.69	1.70	N/A	N/A
Standard Vaporization H°_{vap} (kJ/mol)	42.34	37.80	38.50[a]	20.07[a]
Vapour Pressure (kPa)	7.870	16.90	37.84	429.40

N/A: not applicable (not defined for the mixture); [a]: sourced: [27].

Table 2. Classification of liquids.

Liquid	Can It Be Considered a Petroleum Liquid?	More Appropriate Class
LCO	Yes	Petroleum liquid/petroleum-derived hydrocarbon liquid
NGL	Yes, broadly	Petroleum liquid/natural-gas-derived hydrocarbon liquid
Ethanol	No	Oxygenated organic liquid /alcohol
Methanol	No	Oxygenated organic liquid /alcohol

4.2. Shape of Storage Vessel versus Liquid Volume Retention

The headspaces (the exposed liquid-air interfacial area is considered a geometric proxy for the influence of headspaces on evaporative shrinkage) present in the storage vessels are shown in Table 3. The mass transport between the liquid-vapour space may be influenced by the headspaces available in the storage system. The data set shows an increasing order of headspaces in the designed storage vessels as conical < cuboidal < horizontal cylindrical < vertical cylindrical < spherical vessel. The shrinkage pattern for the cumulative vessel performance across all four liquids shows that the rate of shrinkage was nearly consistent with the headspace trend, as the conical vessel had the least value, while the spherical vessels had the highest value. It was observed that the conical vessel had the highest cumulative retention index, and the spherical vessel the least (Table 4).

Table 3. Headspaces present in storage vessels form Day-1.

Vessel Type	Spherical	Vertical Cylindrical	Horizontal Cylindrical	Cuboidal	Conical
Surface area of the headspace (cm^2)	804	707	228	189	36

Table 4. Summary of cumulative vessel performance across all four liquids.

Vessel	Mean Day-7 Retained Volume (L)	Mean Day-7 Shrinkage (%)	Mean Retained Volume, Days 2 - 7 (L)	Cumulative Retention Index (AUC)
Conical	0.700	30.000	0.798	19.760
Cuboidal	0.522	47.750	0.635	16.195
Horizontally Cylindrical	0.565	43.500	0.683	17.260
Spherical	0.478	52.250	0.595	15.335
Vertically Cylindrical	0.640	36.000	0.734	18.340

Considering the daily retained volume of the organic liquids in the horizontally cylindrical vessel in Figure 3, it is deduced that the organic liquids' retention after daily losses followed the increasing order of NGL < LCO < methanol < ethanol. Similar patterns are observed for vertically cylindrical, spherical, and conical vessels in Figures 4-6, respectively. This shows that the retained volumes of the liquids after daily losses to evaporation are influenced by the shapes of the storage vessels.

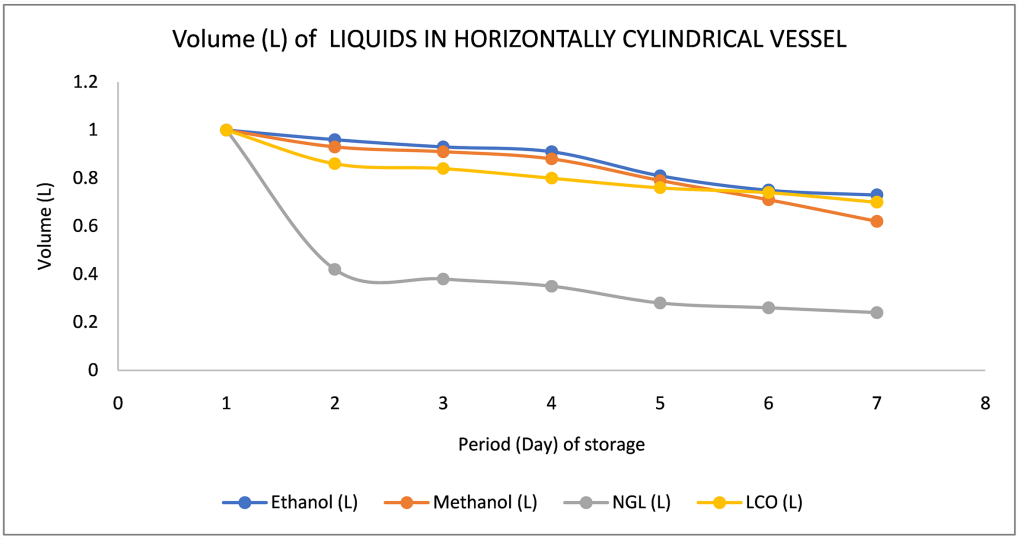

Figure 3. Volume (L) of organic liquids in a horizontally cylindrical vessel during the period of storage.

4.3. Volume Retention and the Competitive Effects of the Intermolecular Force of Attraction, API Gravity, Vapour Pressure, and Polarity of Liquids

Figure 4 for the vertically cylindrical vessel shows that retained volume decreases with time for all four liquids, but at markedly different rates. By day 7, the volume retained was in the following order: NGL < methanol < ethanol = LCO; this showed terminal retained volumes of 0.31, 0.68, 0.78, and 0.79, respectively. This confirmed that NGL is the least retentive liquid by a wide margin, while ethanol and LCO perform best overall. The train of volume retention here is similar to other shapes' storage vessels considered in this work and shows that volume retention

in the vessels is governed primarily by the competition between volatility and cohesive intermolecular attraction, with API gravity and polarity acting as secondary descriptors. The ethanol-methanol comparison is especially instructive. Although both liquids are polar protic alcohols and have a close range of API gravities (48.60 and 46.20 ˚API) and very similar dipole moments (1.69 and 1.70 D), ethanol consistently retains more liquid than methanol after the first few days. This is fully consistent with ethanol's higher standard enthalpy of vaporization (42.34 kJ·mol^{-1}) and lower vapor pressure (7.87 kPa) compared with methanol's 37.80 kJ·mol^{-1} and 16.90 kPa. A higher ΔH_{vap}° implies a stronger net cohesive attraction in the liquid phase, so more energy is required for molecules to escape. At the same time, a lower vapor pressure reduces the thermodynamic driving force for evaporation. Methanol has a slightly higher hydrogen bonding effect than ethanol, while ethanol has larger London dispersion forces than methanol [37] [38].

So, intermolecular forces of attraction (cohesive energy) and volatility are better factors to explain volume retention in alcohols than the slight differences in API gravity and dipole moment (polarity). This interpretation agrees with recent work showing that liquid-phase alcohol behaviour is strongly shaped by hydrogen bonding and local solvation effects [7] [37].

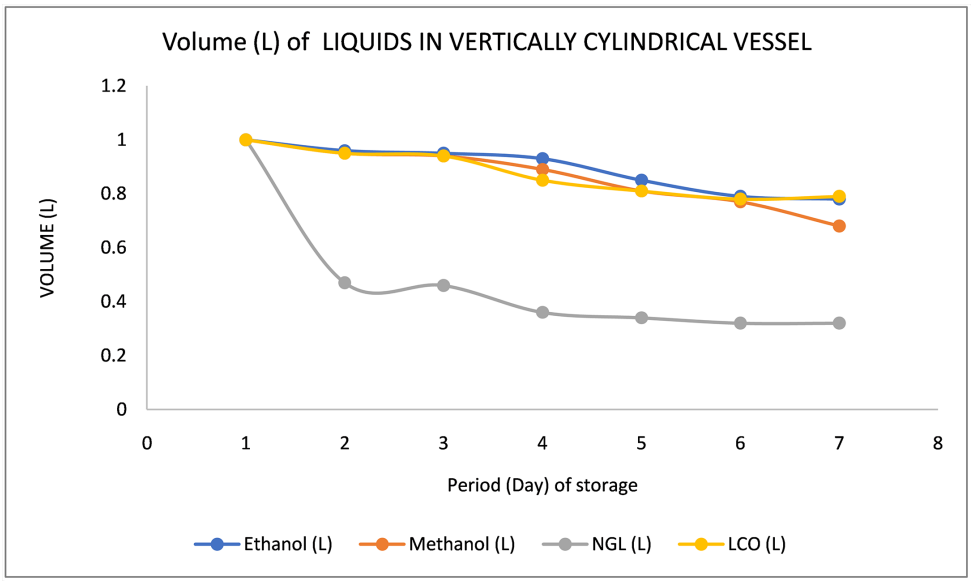

Figure 4. Volume (L) of organic liquids in the vertically cylindrical vessel during the period of study.

The hydrocarbon pair shows a different but complementary pattern. NGL has the highest API gravity (75.7 ˚API) and the lowest assigned enthalpy of vaporization (20.07 kJ·mol^{-1}), together with by far the highest representative vapor pressure (429.40 kPa). Its retained volume drops sharply from 1.00 L on day 1 to 0.46 L on day 2, then to 0.31 by day 7, demonstrating that it is the most evaporation-prone liquid in the set. By contrast, LCO has the lowest API gravity (44.8 ˚API), higher ΔH_{vap}° (38.50 kJ·mol^{-1}) than NGL, and a much lower representative vapor pressure (37.84 kPa) than NGL, and it shows far better retention. So, for the

hydrocarbon mixtures, API gravity contributes to hydrocarbon lightness and volatility distribution, even though it is not itself a direct thermodynamic evaporation parameter.

From the dataset obtained in this study, ethanol and LCO are nearly indistinguishable at day 7 (0.78 vs. 0.79), even though ethanol has the lower vapor pressure and slightly higher cohesive-energy descriptor. This near-convergence suggests that, over the observed period, the final retained volume is not controlled by a single property. Instead, the data support a competitive interpretation based on several properties: ethanol benefits from strong intermolecular attraction and low vapor pressure, whereas LCO benefits from being a heavier hydrocarbon mixture with much lower volatility than NGL and an effective cohesive energy that is still relatively high. The 0.01 L difference between the volumes of ethanol and LCO at day 7 is so small that it should not be overinterpreted; it is inferred that both liquids exhibit high retention relative to methanol and especially NGL, and this was arrived at for somewhat different physicochemical reasons.

Polarity may be best considered here as a qualitative classifier rather than a universal quantitative predictor of retention. Ethanol and methanol are discrete polar molecules with measurable dipole moments, whereas NGL and LCO contain several hydrocarbon mixtures, for which no single molecular dipole moment can be meaningfully assigned.

4.4. Volume Retention and the Competitive Effects of Interfacial Evaporation, API Gravity, and Polarity of Liquids

The data from the spherical vessel in **Figure 5** shows a clear volume retention after 7 days: NGL < methanol < LCO < ethanol, with retained volumes of 0.17, 0.55, 0.59, and 0.60 L, respectively. Expressed as loss from the initial unit volume, this corresponds to about 83% for NGL, 45% for methanol, 41% for LCO, and 40% for ethanol. When the entire 7-day period is considered, the mean retained volumes are about 0.354, 0.757, 0.739, and 0.763 L for NGL, methanol, LCO, and ethanol, respectively, showing that NGL is consistently the least retained liquid. In contrast, ethanol performs best overall, and LCO becomes more competitive toward the end of the test.

From the interfacial standpoint, **Table 5** is consistent with the generic Hertz-Knudsen interpretation that evaporation flux increases with the term $\alpha\left(P_{sat}-P_{v}\right)/2\pi MRT$. The net interfacial flux depends not only on saturation pressure but also on the vapor pressure already established near the interface. So, liquids with high vapor pressure shrink more at early times but may shrink less as the headspace accumulates with more vapor; this explains the rapid reduction of NGL from 1.00 - 0.32 L by day 2 as well as its subsequent slower decline to 0.17 by day 7. In other words, the spherical-vessel behaviour is consistent with an initially strong interfacial driving force followed by progressive vapor-phase moderation, as expected from Hertz-Knudsen-Schrage-type thinking [13] [39].

The vapor-pressure data provide the strongest direct explanation for the extreme ends of the retention trend. NGL has the highest vapor pressure (429.40 kPa), and it also shows the lowest retention throughout the experiment. Ethanol has the lowest vapor pressure (7.87 kPa) and the highest day-7 retained volume. There is an inverse relationship between vapor pressure and retained volume, and this is consistent with the literature on evaporation, as vapor pressure is considered one of the principal thermodynamic controls on liquid loss [5] [11].

The methanol-ethanol comparison further shows that interfacial evaporation and vapor pressure remain more decisive than API gravity alone for the pure liquids. Although their API gravities are very close (48.6 and 46.2 ˚API) and both are single-component oxygenated liquids, methanol retains less volume than ethanol over the 7 days. That difference aligns with the much larger adopted methanol interfacial flux (molar evaporation flux) parameter of 756.92 and 8.82 $m^{-2}\cdot s^{-1}$ for methanol and ethanol, respectively, and with methanol's higher vapor pressure of 16.90 kPa compared to that of ethanol, 7.87 kPa. The Hertz-Knudsen parameters buttress that the observed retention trend is best interpreted as a process controlled by volatility [5] [38].

Table 5. Interfacial evaporation parameter of liquids.

Substance	α	P_{vap} (Pa)	M (kg/mol)	$\sqrt{2\pi MRT}$	J ($m^{-2}\cdot s^{-1}$)
Methanol	1	16900	0.03204	22.33	756.92
Ethanol	0.03	7870	0.04607	26.77	8.82
LCO	N/A	37840	0.1142	42.15	Higher than Methanol
NGL	N/A	429400	0.0581	30.07	Higher than LCO

For the hydrocarbon mixtures (NGL and LCO), API gravity (**Figure 7**) is more useful, but still only as a secondary, bulk descriptor. NGL has the highest API gravity (75.7 ˚API), meaning it is the lightest hydrocarbon fluid in the set, whereas LCO has the lowest (44.8 ˚API) and is therefore the densest/heaviest of the two hydrocarbon liquids.

A technically important point is that the LCO-methanol crossover shows why no single property can explain the spherical-vessel data completely. **Table 5** qualitatively places LCO above methanol in interfacial-evaporation tendency, yet the measured day-7 retained volume of LCO (0.59 L) is still higher than that of methanol (0.55 L). This apparent inconsistency is not surprising, because the LCO and NGL values are based on proportionality of the driving force (vapour pressure), and α is unavailable for these multicomponent fluids, which may turn otherwise. In real hydrocarbon mixtures, evaporation progressively changes composition, lowers the abundance of the most volatile fractions, and shifts the effective driving force with time.

This also informs that the spherical storage vessel's dataset aligns with the fact that API gravity provides a useful compositional context for the hydrocarbon liq-

uids rather than a stand-alone predictor of loss volume retention, while the primary controlled parameters in this set are interfacial evaporation and vapor-pressure-driven volatility. NGL shows the worst retention because its very high vapor pressure and light hydrocarbon character create the strongest evaporative tendency. Ethanol shows the best retention because of its low vapor pressure and very low adopted interfacial flux.

It is inferred that LCO retains relatively well because its higher hydrocarbon content offsets less volatile [5] [11].

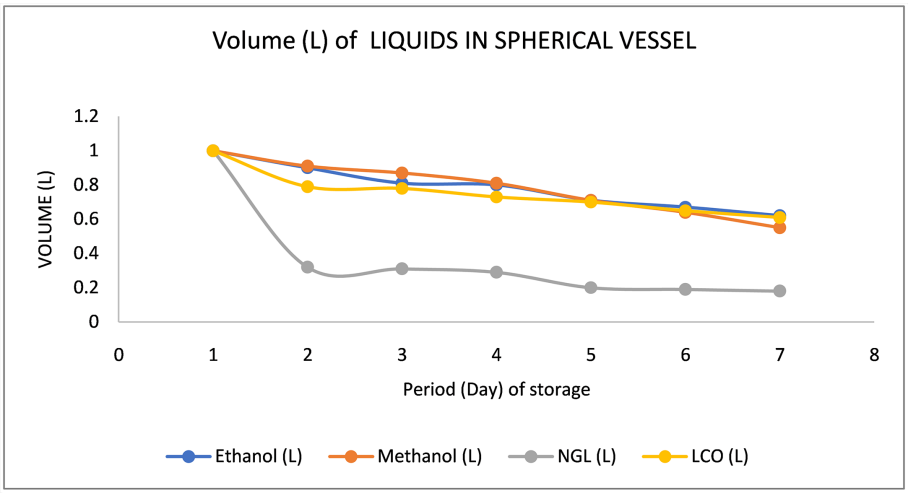

Figure 5. Volume (L) of organic liquids in the spherical vessel during the period of study.

4.5. Volume Retention and the Competitive Effects of Gas-Phase Diffusion and Surface Area of Headspace

Using Equation (18), and taking the headspace surface area as the effective exposed area, A, while keeping h_m and $\left(Y_{\upsilon,i} - Y_{g,\infty}\right)$ constant, the predicted evaporation loss rate becomes directly proportional to Aρ. Under this simplification, vessel geometry is expected to exert a first-order control on liquid loss as a larger headspace area results in a larger effective mass-transfer area. In contrast, higher liquid density increases the mass-loss term. Previous work has already mentioned that exposed area and gas-side transport are key determinants of open-surface evaporation [5] [14].

The geometry ranking of A is spherical (0.0804) > vertical cylindrical (0.0707) > horizontal cylindrical (0.0228) > cuboidal (0.0189) > conical (0.0036). Because h_m and $\left(Y_{\upsilon,i} - Y_{g,\infty}\right)$ are held constant, this same ranking applies to the theoretical mass-loss tendency for each liquid. Relative to the conical vessel, the geometric loss potential is about 22.3 times higher in the spherical vessel, 19.6 times higher in the vertical cylindrical vessel, 6.3 times higher in the horizontal cylindrical vessel, and 5.3 times higher in the cuboidal vessel. Thus, from the gas-phase diffusion model alone, the conical vessel yields the highest retention, and the spherical vessel, the lowest. These show that a larger evaporative area enhances mass transfer, consistent with other studies [5] [14].

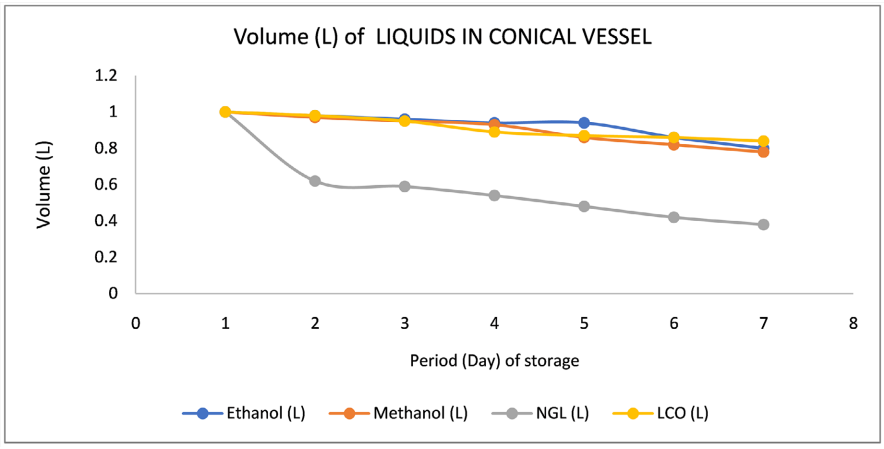

Figure 6. Volume (L) of organic liquids in the conical vessel during the period of study.

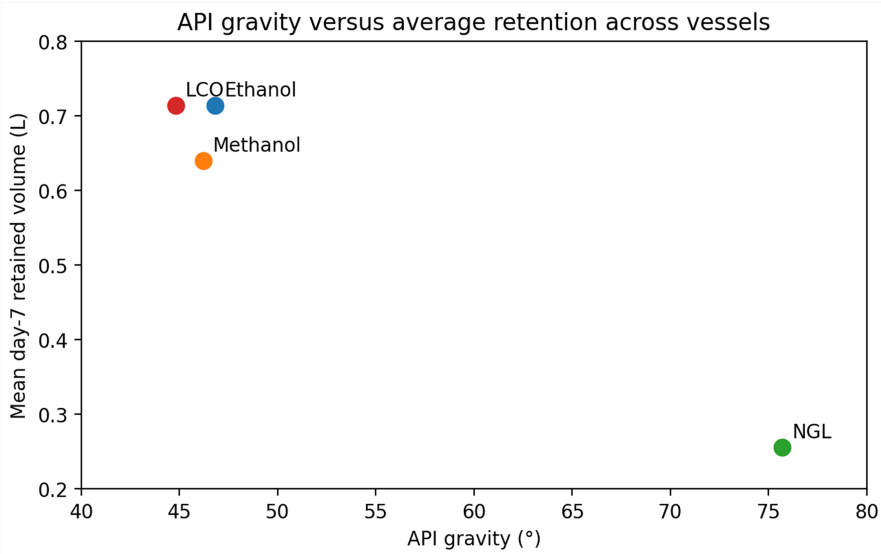

Figure 7. API gravity versus average day-7 retention across the five vessels.

The day-7 heatmap in Figure 8 supports this first-order area effect at the two extremes. Averaged across the four liquids, the conical vessel gives the highest day-7 retained volume (0.700), whereas the spherical vessel gives the lowest (0.478). This inverse relationship between retention and headspace area is especially clear for every individual liquid: ethanol is retained best in the conical vessel (0.80) and worst in the spherical vessel (0.60); methanol shows the same pattern (0.78 vs. 0.55); NGL likewise (0.38 vs. 0.17); and LCO also (0.84 vs. 0.59). These results emphasize the need to consider other factors, such as the mass-transfer coefficient and vapour mass fraction, so as to obtain sufficient data for real-life applications [14].

However, the middle-order geometry trend is not fully explained by headspace area alone. If the area in the evaporation rate (mass loss rate) of Equation (18) were the only controlling factor, then retention order should be the exact reverse of area, namely conical > cuboidal > horizontal cylindrical > vertical cylindrical >

spherical. The measured average retention instead follows conical > vertical cylindrical > horizontal cylindrical > cuboidal > spherical. The unexpectedly good performance of the vertical cylindrical vessel, despite its much larger area than the horizontal and cuboidal vessels, indicates that real gas-phase diffusion is not controlled by A alone, even though A is the dominant term in the present simplification. This is where the gas-side mass-transfer coefficient (h) expression in Equation (19) becomes important, as it shows that the gas-side mass-transfer coefficient also depends on the Sherwood number (Sh), the diffusion coefficient ($D_{\upsilon,g}$), and the characteristic length (L). The term for the liquid's density in Equation (18) introduces a second competitive effect. Keeping geometry for a given measured evaporation rate, and area constant, the driving force, h_m is inversely proportional to ρ and assessing retention by density (ρ), we have the decreasing order of methanol (791 kg·m^{-3}) > ethanol (784 kg·m^{-3}) > LCO (686 kg·m^{-3}) > NGL (564 kg·m^{-3}), so the simplified gas-phase model predicts the greatest mass-loss tendency NGL and the least for methanol. Also, the retained volumes in Figure 6, for the volume of liquids retained in the conical vessel, as well as the more elaborate display in Figure 8, the heatmap, buttresses from the liquid-level trend for day-7 retention, with NGL always retained least and ethanol/LCO most. This means the effects of molecular thermodynamics outweigh those of density alone. Even so, within the present context, the gas-phase model remains useful because it explains why geometry strongly separates retention performance, even when the liquid ranking itself is governed by additional properties beyond the constant-h_m, constant-($Y_{\upsilon,i} - Y_{g,\infty}$) assumption; this is the reason methanol could not be the most retained liquid in practice, in this study [11] [12].

So, the surface area of headspace, which is a function of the vessel's geometry, plays a major role in volume retention after evaporation.

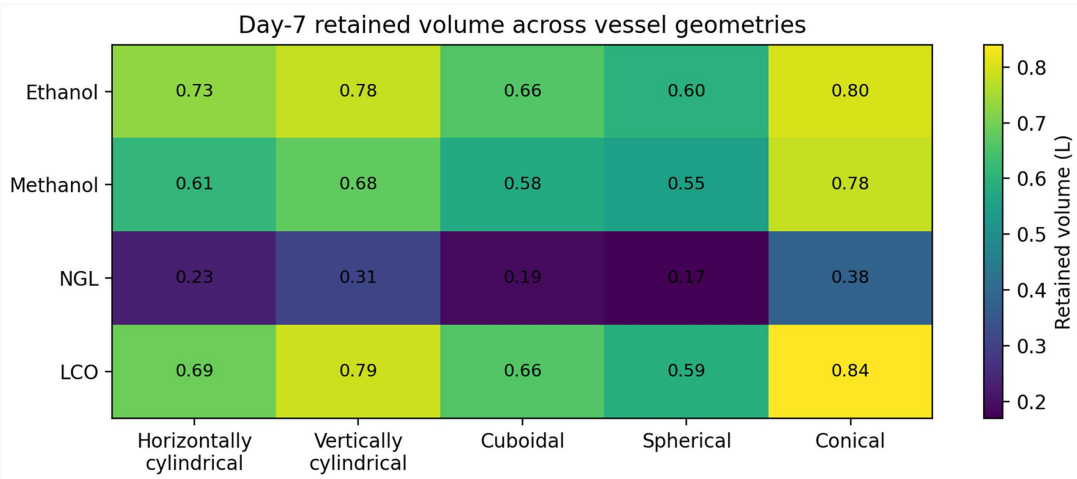

Figure 8. Heatmap of day-7 retained volume across liquid-geometry combinations.

5. Conclusions

This study has identified that liquid polarity has minimal influence on liquid re-

tention during evaporative losses. Intermolecular cohesion and phase-equilibrium behaviour are modified; however, for multicomponent petroleum liquids such as LCO and NGL, the experimentally observed shrinkage is more strongly governed by volatility distribution, vapor pressure, and external mass-transfer conditions than by polarity alone.

It was realised that API gravity functioned to interpret hydrocarbon mixtures, and that polarity mainly distinguished alcohols from predominantly nonpolar hydrocarbon fluids. The very poor retention of NGL is explained by its extremely high volatility and low cohesive energy; the lower retention of methanol relative to ethanol is explained by its higher vapor pressure and lower ΔH_{vap}°; and the strong retention of LCO reflects the comparatively less volatile nature of the heavier hydrocarbon mixture. So, it was inferred that the retained volume is controlled by the competitive interaction of volatility, cohesive attraction, and bulk liquid character, rather than by API gravity or polarity alone.

The dataset generated in this work supports the conclusion that retained volume in the varied vessel geometries reflects the competitive interaction of kinetic interfacial evaporation, intrinsic vapor pressure, and bulk hydrocarbon lightness (deduced from API gravity, rather than the action of any single parameter in isolation). On the other hand, the departure of the vertical cylindrical vessel from the pure area-based order shows that gas-phase diffusion and convection compete with simple area effects. The results support the conclusion that day-7 retained volume across the five vessel types is governed by a competitive interaction between available headspace area and gas-side mass-transfer behaviour, rather than by headspace area alone.

Authors' Contributions

Gideon Mudiaga Efetobor: Writing—Original Draft, Formal Analysis, Conceptualisation. Idongesit Effiong Ekpo: Writing—Review & Editing, Investigation, Formal Analysis. Ikodia Orji: Resources, Validation, Writing—Review & Editing. Ozioma Achugasim: Validation, Supervision, Conceptualisation. Pereware Adowei: Investigation, Methodology, Formal Analysis.

Acknowledgements

The authors are thankful to the Department of Pure and Industrial Chemistry, the School of Science Laboratory and Technology, and Ideal Geochem and Environmental Services Limited for providing laboratory support and assisting with sampling during this study.

Data Availability

The other data that are not included will be provided on request.

Conflicts of Interest

The authors declare no conflicts of interest regarding the publication of this paper.

References

[1] Elsevier, B.V. (2026) Vapor Pressure. ScienceDirect Topics. https://www.sciencedirect.com/topics/earth-and-planetary-sciences/vapor-pressure

[2] U.S. Energy Information Administration (2026) Table Definitions, Sources, and Explanatory Notes: Petroleum Refining & Processing-Qualities of Crude Oil Input. https://www.eia.gov/dnav/pet/tbldefs/pet_pnp_crq_tbldef2.asp

[3] McGrattan, K.B., Hostikka, S., Floyd, J.E., Baum, H.R. and Rehm, R.G. (2007) Fire Dynamics Simulator (Version 5): Technical Reference Guide (NIST Special Publication 1018-5). National Institute of Standards and Technology.

[4] Persad, A.H. and Ward, C.A. (2016) Expressions for the Evaporation and Condensation Coefficients in the Hertz-Knudsen Relation. *Chemical Reviews*, **116**, 7727-7767. https://doi.org/10.1021/acs.chemrev.5b00511

[5] Aragón, H. and Mata-Segreda, J.F. (2023) Evaporation Kinetics of Liquid Mixtures and Safe Handling. *ACS Chemical Health & Safety*, **30**, 54-62. https://doi.org/10.1021/acs.chas.2c00070

[6] International Union of Pure and Applied Chemistry (2025) Raoult's Law. In: *IUPAC Compendium of Chemical Terminology*, 5th Edition. https://goldbook.iupac.org/terms/view/15349

[7] Jorge, M., Nunes, R., Grilo, I.A., Cordeiro, M.N.D.S. and Lopes, J.N.C. (2022) The Dipole Moment of Alcohols in the Liquid Phase and in Solution. *Journal of Molecular Liquids*, **361**, Article 119636.

[8] Shishkova, I., Stratiev, D., Kolev, I.V., Nenov, S., Nedanovski, D., Atanassov, K., *et al.* (2022) Challenges in Petroleum Characterization—A Review. *Energies*, **15**, Article 7765. https://doi.org/10.3390/en15207765

[9] Spange, S. (2024) Polarity of Organic Solvent/Water Mixtures Measured with Reichardt's B30 and Related Solvatochromic Probes—A Critical Review. *Liquids*, **4**, 191-230. https://doi.org/10.3390/liquids4010010

[10] Waghorne, W.E. (2024) Solvent Polarity/Polarizability Parameters: A Study of Catalan's SPPN, Using Computationally Derived Molecular Properties, and Comparison with Π and Et(30). *Liquids*, **4**, 163-170. https://doi.org/10.3390/liquids4010008

[11] Zhang, C., Sun, H., Fu, P., Hu, Y., Huang, X. and Zhao, D. (2026) A Systematic Literature Review on the Evaporation Loss Mechanisms and Local Diffusion Characteristics of Volatile Organic Compounds (VOCs) from Petrochemical Storage Tanks. *Journal of Loss Prevention in the Process Industries*, **99**, Article 105801. https://doi.org/10.1016/j.jlp.2025.105801

[12] Huang, W., Wang, S., Jing, H., Wang, C., Sun, X., Zhou, N., *et al.* (2020) A Calculation Method for Simulation and Evaluation of Oil Vapor Diffusion and Breathing Loss in a Dome Roof Tank Subjected to the Solar Radiation. *Journal of Petroleum Science and Engineering*, **195**, Article 107568. https://doi.org/10.1016/j.petrol.2020.107568

[13] Poós, T. and Varju, E. (2024) Review for Convection Based Evaporation of Open Liquid Surface and Equations of Evaporation Rate. *International Communications in Heat and Mass Transfer*, **157**, Article 107755. https://doi.org/10.1016/j.icheatmasstransfer.2024.107755

[14] Wijnhorst, R., Van der Sloot, F., Pel, L. and Shahidzadeh, N. (2024) Effect of Evaporative Surface Area on Salt Efflorescence and Subflorescence Formation in a Given Porous Material. *Physical Review Applied*, **21**, Article No. 064055. https://doi.org/10.1103/physrevapplied.21.064055

[15] Kumar, L. and Sleiti, A.K. (2024) Modeling and Analysis of Effect of Various Tank

Geometries and Relief Pressure on Liquid Hydrogen (LH2) Boil-Off Losses. *Energy Proceedings*, **44**, Article 11076.

[16] ASTM International (2024) Standard Test Method for Density, Relative Density, or API Gravity of Crude Petroleum and Liquid Petroleum Products by Hydrometer Method (ASTM D1298-24). ASTM International.

[17] Okwudili, O.J., Osuji, L.C., Ekpo, I. and Upua, P.U. (2025) Removal of Heavy Metals from Spent Automobile Engine Oil Using Oil Palm Biomass. *Journal of Applied Chemical Science International*, **16**, 41-51. https://doi.org/10.56557/jacsi/2025/v16i19157

[18] Šegatin, N., Pajk Žontar, T. and Poklar Ulrih, N. (2020) Dielectric Properties and Dipole Moment of Edible Oils Subjected to 'Frying' Thermal Treatment. *Foods*, **9**, Article 900. https://doi.org/10.3390/foods9070900

[19] Kremer, F. and Tress, M. (2025) Dielectric Spectroscopy: Yesterday, Today and Tomorrow. *Applied Sciences*, **15**, Article 6954. https://doi.org/10.3390/app15136954

[20] American Petroleum Institute (2021) Manual of Petroleum Measurement Standards (MPMS), Chapter 3.1A: Standard Practice for the Manual Gauging of Petroleum and Petroleum Products (Consolidated Version of 3rd Edition, Incorporating Errata 1).

[21] Autodesk (2024) What's New in AutoCAD 2024. Autodesk Help.

[22] García-G, D., Barco-Burgos, J., Chaparro, J., Eicker, U., Cárdenas D.R, J. and Saldaña-Robles, A. (2024) Analyzing Joint Efficiency in Storage Tanks: A Comparative Study of API 650 Standard and API 579 Using Finite Element Analysis for Enhanced Reliability. *International Journal of Pressure Vessels and Piping*, **207**, Article 105113. https://doi.org/10.1016/j.ijpvp.2023.105113

[23] ASTM International (2021) ASTM E542-01(2021): Standard Practice for Calibration of Laboratory Volumetric Apparatus. https://doi.org/10.1520/E0542-01R21

[24] American Petroleum Institute (2016) Petroleum Measurement Standards: Chapter 19, Evaporation Loss Measurement (Catalog Listing). API Publications Catalog. https://www.api.org/~/media/files/publications/2018_catalog/2018_pubs_catalog_final_pm.pdf

[25] International Organization for Standardization (2022) ISO 7507-2:2022 Petroleum and Liquid Petroleum Products-Calibration of Vertical Cylindrical Tanks-Part 2: Optical-Reference-Line Method or Electro-Optical Distance-Ranging Method. 3rd Edition, ISO.

[26] International Organization for Standardization (2023) ISO 4266-1:2023 Petroleum and Liquid Petroleum Products-Measurement of Level and Temperature in Storage Tanks by Automatic Methods-Part 1: Measurement of Level in Atmospheric Tanks. 2nd Edition, ISO.

[27] National Institute of Standards and Technology (2026) Ethanol. NIST Chemistry WebBook (SRD 69). https://webbook.nist.gov/cgi/cbook.cgi?ID=C64175&Type=HVAP

[28] National Institute of Standards and Technology (2026) Methyl Alcohol. NIST Chemistry WebBook (SRD 69). https://webbook.nist.gov/cgi/cbook.cgi?ID=C67561&Type=HVAP

[29] ASTM International (2023) ASTM D2879-23, Standard Test Method for Vapor Pressure-Temperature Relationship and Initial Decomposition Temperature of Liquids by Isoteniscope. ASTM International.

[30] Ibezim-Ezeani, M.U., Obi, C., Ekpo, I.E., Victor-Oji, C. and Tamunosaki, D. (2023) Basic Physical Chemistry. 1st Edition, CEL WIL.

[31] eralytics GmbH (2021) Crude oil Vapor Pressure Testing: Why a Higher Shaker Speed

Improves the Accuracy of ASTM D6377.
https://eralytics.com/news/crude-oil-vapor-pressure-testing-why-higher-shaker-speed-improves-accuracy-of-astm-d6377/

[32] ASTM International (2020) ASTM D6377-20, Standard Test Method for Determination of Vapor Pressure of Crude Oil: VPCRx (Expansion Method) ASTM International.

[33] Goss-Sampson, M.A. (2025) Statistical Analysis in JASP: A Guide for Students. 7th Edition, JASP.
https://jasp-stats.org/wp-content/uploads/2025/07/Statistical-Analysis-in-JASP-A-guide-for-students-2025.pdf

[34] Ragozzino, E., Bortolani, S., Di Pietro, L., Orecchini, E., Papait, A., Nanni, S., *et al*. (2026) RNA Cargo Profiling of Muscle Extracellular Vesicles Identifies Candidate Biomarkers of Disease Activity and Muscle Degeneration in FSHD. *Journal of Translational Medicine*, **24**, Article 332. https://doi.org/10.1186/s12967-026-07794-y

[35] Sörgel, F., Thyroff-Friesinger, U., Vetter, A., Vens-Cappell, B. and Kinzig, M. (2009) Bioequivalence of HX575 (Recombinant Human Epoetin Alfa) and a Comparator Epoetin Alfa after Multiple Intravenous Administrations: An Open-Label Randomised Controlled Trial. *BMC Clinical Pharmacology*, **9**, Article 10.
https://doi.org/10.1186/1472-6904-9-10

[36] Kamal, I., Salih, N.M. and Martyushev, D.A. (2023) Correlations between Petroleum Reservoir Fluid Properties and Amount of Evolved and Dissolved Natural Gas: Case Study of Transgressive-Regressive-Sequence Sedimentary Rocks. *Journal of Marine Science and Engineering*, **11**, Article 1891. https://doi.org/10.3390/jmse11101891

[37] American Chemical Society (2016) The Key Role of Hydrogen Bonding.
https://www.acs.org/content/dam/acsorg/education/publications/ch8.pdf?utm

[38] Higginbotham, C. (2021) Intermolecular Forces. In: *Introductory Organic Chemistry*, 56-66.
https://openoregon.pressbooks.pub/introductoryorganic/chapter/intermolecular_forces/

[39] Spaska, O.A., Daszykowski, M. and Bushuev, Y.G. (2024) Evaluation of Evaporation Fluxes for Pesticides and Low Volatile Hazardous Materials Based on Evaporation Kinetics of Net Liquids. *ACS Omega*, **9**, 18617-18623.
https://doi.org/10.1021/acsomega.4c01405